Check for
updates

Study on Microstructure and Anti-Corrosion Property of Stainless Steel Particles Deposition on Ti–6Al–4 V Substrate using Laser Cladding Technique

N. Jeyaprakash[1] · **Mahendra Babu Kantipudi[2,3]** · **Che-Hua Yang[1]**

Abstract

In the present study, the Stainless Steel (SS420) particles is deposited on Ti–6Al–4 V (Ti-64) substrate using laser cladding process. The cladded structure and hardness were analysed through Field Emission Scanning Electron Microscopy (FESEM) and Nanoindenters, respectively. Then, the corrosion behaviour of the cladded surface was analysed with polarization test and electrochemical impedance method with different testing hours (0, 18 and 42 h). Further, the roughness of the corroded surface was measured using laser confocal microscopy. Result showed that the laser cladded surface shows with three structures namely, coaxial dendrites, columnar dendrites and cellular dendrites. The cladding nanohardness (10.58 GPa) was higher while compared with base (4.53 GPa) and interface regions (5.89 GPa). Corrosion current density at 18 h test specimen is lower than that at 0 h and 42 h test specimen and improved the corrosion resistance by forming the passive layer at 18 h test specimen. Moreover, lesser roughness was noticed at 18 h test specimen due to reduced corrosion rate.

Keywords Ti–6Al–4 V · SS420 cladding · Nanohardness · Electrochemical corrosion · Roughness

✉ N. Jeyaprakash
prakash84gct@gmail.com; prakash@ntut.edu.tw

Mahendra Babu Kantipudi
mahendra.k4u@gmail.com

Che-Hua Yang
chyang@ntut.edu.tw

[1] Graduate Institute of Manufacturing Technology, National Taipei University of Technology, Taipei 10608, Taiwan

[2] Department of Vehicle Engineering, National Taipei University of Technology, Taipei 10608, Taiwan

[3] Department of Mechanical Engineering, Vishnu Institute of Technology, Bhimavaram, Andhra Pradesh, India

Abbreviations

SS420   Stainless Steel 420
Ti-64   Ti–6Al–4 V
PVD   Physical Vapour Deposition
HAZ   Heat-Affected Zone
FESEM   Field Emission Scanning electron microscopy
EDS   Energy Dispersive Spectroscopy
Yb   YAG: Ytterbium Doped Yttrium Aluminum Garnet
EDM   Electrical Discharge Machining
GSM   Grams Per Square Metre
EIS   Electrochemical Impedance Spectroscopy
CPE   Constant Phase Element

Introduction

Owing to high strength at low weight, corrosion performance, low cost, high-temperature capability and biocompatibility, titanium alloys are emerging as important material in engineering and medical applications. Titanium-based alloys can be classified as α, β and α-β alloys. Ti–6Al–4 V (Ti64) is an α-β alloy that is a frequently used material in automobile, aerospace, biomedical and marine applications. Aluminium gives α phase stability and vanadium gives β phase stability. Hence this alloy possesses good mechanical properties [1]. On the other hand, the wear resistance of Ti-64 is not up to the mark. Even though titanium has good corrosion resistance, it has a drawback of erosion-corrosion. Budinski [2] performed a study and concluded that titanium is inclined to adhesive wear against other materials. The oxide layer formed on titanium alloy is easily destroyed in erosion conditions. Due to these reasons the applications of titanium alloys are reduced.

Therefore, it is very essential to enhance the surface level properties by adopting surface treatments. Recently, the surface treatments such as Physical Vapour Deposition (PVD), thermal spraying, gas nitriding, electroplating, laser treatments etc. is using to improve the surface level properties. Among those, by using PVD technique, fine surface cladding with good mechanical and tribological properties can be produced [3]. However, separation of coating from a substrate takes place during long usage. Thermal spraying is another technique that improves or re-establishes the surface of a solid material [4]. However, it is a complicated and expensive operation. Gas nitriding is a surface hardening technique in which heat is used to impinge nitrogen gas into the surface of the metal [5]. However, the hardness enhancement using this method is limited. Therefore, the route of study has changed from outdated hardening processes to new laser based technologies.

The surface treatment with laser turns out to be more extensive in the current mechanical industries. It is one of the reliable techniques to achieve surface properties more effectively. Using this laser treatment technique, material hardening, alloying, surface texturing and cladding can be achieved [6–9]. Laser cladding is one of the advanced technique to deposit the powder particles on the base metal surface. Moreover, the alloy particles can impinge near the base material through

better quality and a small amount of dilution. Due to this reason, the bonding between this coating and base metal is very promising. Therefore, researchers have paid attention towards the laser cladding method to reach an improved surface quality. In this process, the base metal is heated and then the metal powder is deposited on it [10]. It is becoming much popular due to less energy intake, layer thickness flexibility (50 μm–2 mm), robust cladding-substrate metallurgical bonding, fine microstructure, and low distortion [11].

The pre-blended alloy powders have been well-known as key content in improving the tribological properties of the metallic surfaces. In this way, to improve the wear resistance of the Ti-64, hard alloy powders are necessary. Cobalt, nickel and steel nanoparticles are a few commercially existing and applicable hard alloys. Shasha [12] performed cobalt-based coating on titanium alloy to reduce the wear to 1/12 of the base material wear. Lu [13], have been performed nickel-based coating on Ti-64 substrate and improved the tribological properties. Jeyaprakash et al. [14] deposited SS420 and Colmonoy 5 (nickel-based alloy) particles over SS410 to enhance the tribological properties. Wang et al. [15] investigated the wear performance of stainless steel cladding and emphasized the effect of molybdenum content on wear and corrosion resistance. The steel-based powder is the best among the above powders because of high hardness at a low cost. Jeyaprakash and Yang [16] cladded SS420 powder on Ti-64 to improve the dry sliding wear properties.

Corrosion is an essential failure type normally happening in the engineering equipment, mainly the impels, regulators and other types of machinery of naval and energy generation industries. Garcia [17] improved the corrosion properties of the magnesium alloy using steel particle coating. It is very essential to study the corrosion performance of laser cladding, to use in various environmental conditions. Cabrini et al. [18] studied the corrosion performance of nickel-based alloy which is produced by laser powder bed. Feng, et al. [19] studied the corrosion behaviour of laser cladding CrCoNi medium entropy alloy coating and found that the cladding shows outstanding corrosion resistance. Shen et al. [20] discussed the effect of laser cladding speed on the microstructure and eventually corrosion resistance of coatings. Mohammad [21] analysed the corrosion behaviour of Ti-64 cladded on Ti-64 substrate. The previous literature showed that no preceding studies have deliberated on the corrosion performance of SS420 laser cladding on Ti-64 substrate.

From this literature, it can be seen that the laser cladding method can improve the mechanical and wear properties. However, the corrosion behaviour of laser cladded SS420 on a Ti-64 substrate at various time intervals was not studied. Along with their corroded morphology and surface roughness also have not been evaluated yet. Therefore, this work has attempted to study the microstructure and corrosion performance of laser cladding SS420 on a Ti-64 substrate. SS420 powder was coated on the Ti-64 substrate with a high-power Yb: YAG disc laser. Considering the fact that Ti-alloys exhibit poor corrosion resistance at Cl concentration, NaCl-based corrosion tests were conducted. Field Emission Scanning electron microscopy (FESEM) and Energy Dispersive Spectroscopy (EDS) were used to reveal the microstructural and elemental data analysis. Electrochemical studies were conducted to understand the corrosion potential and resistance of the cladding.
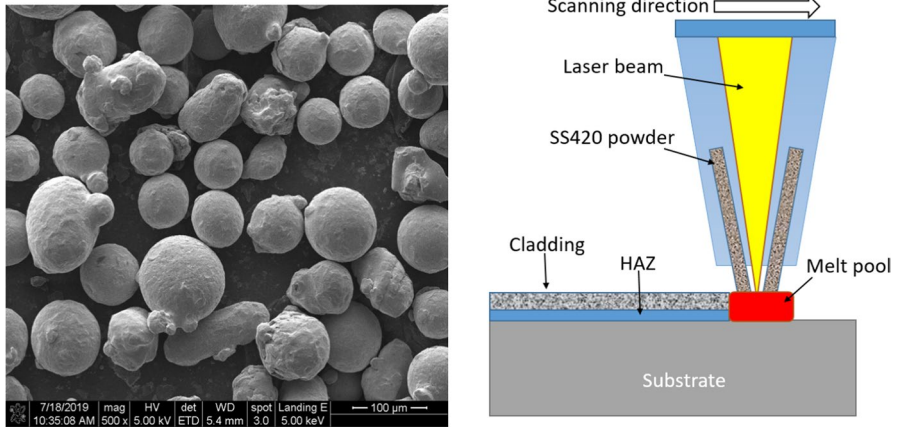
Fig. 1 (**a**) FESEM of as-received SS420 particles, (**b**) Schematic of laser cladding process

Table 1 Chemical composition of SS420 powder and Ti-64 plate [16]

Specimens	Ti	Cr	Fe	Al	C	Si	Mo	Mn	V
SS420	–	14.1	Bal	–	0.17	1.02	–	0.97	–
Ti-64	Bal	0.008	0.121	5.87	0.342	–	0.006	–	3.89

Experimental Procedure

Materials Preparation

Commercially available Ti64 plate was purchased from the market. Then, acetone was used to clean the surface of the base material. Then, the surface roughness was increased to 6 microns using sandblasting to achieve a high bonding between coating and base material. The shape and size of the SS420 powder elements were studied by using FESEM images. Figure 1(a) shows the morphology of the SS420 powder. Particles are having a spherical shape and a typical size of 26–130 microns. Table 1 provides the chemical composition of SS420 powder and Ti-64.

Laser Cladding Setup

The parameters of the cladding process namely flow rate of particle, power and speed of the scanning affect the quality of the coating. Therefore, optimal parameters of cladding as listed in Table 2 were used to clad SS420 particles on a Ti-64 plate using a 4 kW Yb: YAG disc laser (Ytterbium Doped Yttrium Aluminum Garnet). Figure 1(b) shows the schematic of laser cladding setup. After cladding, the samples were taken out and machined using wire Electrical Discharge Machining (EDM) process. The specimen with dimensions of 10 mm^3 was machined for microscopic and corrosion analysis. Then, the

Table 2 Optimal laser cladding parameters

Power	100 W
Speed of Scanning	600 mm/min
Spot size	3.5 mm
Feed rate	7 g/min
preheating	150 deg
overlapping	50%
gas of shielding (argon)	25 lpm
Powder carrier gas (argon)	6 SD@1 bar

samples were polished by emery papers with grades ranging from 340 to 3000 Grams Per Square Metre (GSM) and diamond polishing. Then, the solution of Tetraoxochromic acid (2%) and deionized water was applied as an etchant to expose the microstructure of the specimen. The microstructural characterization of the cross-sections of selected specimens was carried out by Field Emission scanning electron microscopy (FESEM).

Corrosion Test

Electrochemical corrosion test was performed at atmospheric temperature. A liquid of 3.5 wt.% of NaCl and 100 ml deionized water was used as a medium for corrosion test. This test setup is a flat cell in which the workpiece, platinum and AgCl are the three electrodes. The test sample was kept firmly beside a Teflon circular plate with a round opening region to allow the sample surface to electrolytic medium. Then, the sample was dipped in the corrosive solution and allowed a 30 min stabilization period at open-circuit conditions. Then the cell was repeatedly polarized by varying the potential from 0.05 V to 1.2 V with a speed of 1 mV/S. The I-current and the E-current are measurements of corrosion current and the potential of corrosion respectively. They were projected by the Tafel extrapolation technique for the periods of 0 h, 18 h and 42 h on the cladded sample. Electrochemical Impedance Spectroscopy (EIS) was used for the estimation of the anti-corrosion performance of cladding. An equivalent circuit was used to get EIS fields, such as the film capacitance, resistance of the NaCl medium and polarization resistance. Measurements were taken at several frequencies ranging from 10^{-2} to 10^{6} Hz. NOVA software was used for curve fitting and obtaining Nyquist and bode plots. Subsequently, the specimens were washed with alcohol, dried out in the air. Then the surface morphology and element information of the corroded samples were scanned. Further, the roughness of the corroded surface was measured to analyse the effect of corrosion.

Results and Discussion

Microstructure Examination

It is important to study the cladding surface microstructure to understand the quality of the coating uniformity and defects. Therefore, the developed cladding's

microstructure examination was performed with the FESEM. As seen in Fig. 2(a), cladding, heat-affected zone (HAZ) and substrate regions were captured. It can be observed that a good bonding was established between the base and coating materials; the coating is dense, free from cracks and well adhered. This is due to the heat source controlled properly by optimizing the laser parameters and eventually reduced the possibility of defects. As per the available temperature and solidification rate, three different structures were formed namely, cellular dendrites, equiaxed dendrites and needle like lengthy structure [Fig. 2(a-d)]. It is observed that the structure at the interface region showed with lengthy needle structure. The cladding regions display martensite dendrites through the cladding deposition due to constitutional undercooling. The laser power melts the base material and SS420 particles to create the molten pool, Further, the laser source moves to nearby region, the melted alloy powders begin to solidify and created the dendrite structure. Further, the cooling rate (R) mainly related to Temperature gradient (G). While minimizing the G/R ratio, the structure can be changed to cellular to dendrite. In addition to that the substrate always works as a heat sink to interface region with minimum time of solidification (t) and maximum temperature gradient (TG). This needle-shaped and fine grain structure act against the crack formation and improve the corrosion resistance.
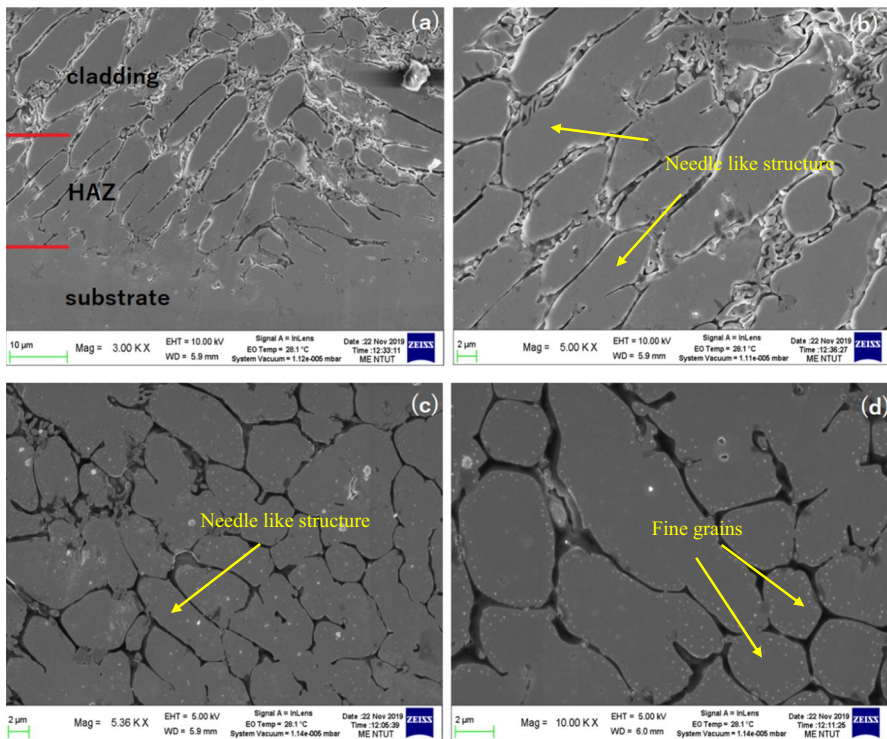

Fig. 2 (**a**) FESEM showing with three various regions namely, cladding, HAZ, and substrate regions, (**b**) magnified view of HAZ, (**c**) cladding center region, and (**d**) magnified view of the cladding center region

Moreover, it is vital to study the interface of the cladding to verify its attachment strength. Generally, the cladded layer can be skinned off due to fewer bond properties and the probability for delamination is there due to the thermal disparity. Also, there is a possibility for cracks because of the fragile manner of intermetallic components. The thickness of the coating has an important effect on the toughness of the coating. Large thickness may increase the brittleness of the interface region. The coating thickness in this study is 627.655 ± 08 l µm, which is minimum. Therefore, there is no possibility of a crack in the interface area of the coating. Figure 2(b) displays the magnified view of HAZ. Moreover, the cladding area is showing Fe in the phase of martensite on the surface of the cladding that can defend the surface from the external loads.

Nanohardness Study

Hardness is an important property that can influence the tribological properties of the material. Thus, the nanoindentation test was conducted to know the hardness trends. Figure 3(a) shows the indentation load-unloading profiles of laser cladding specimens at three distinct regions, i.e., cladded region, HAZ and the substrate. The higher depth of indentation means the lower hardness. As indicated in the figure, the indentation depth at the peak load (1500 µN) is approximately 75 nm at the substrate region, 60 nm at the interface and 40 nm at the surface of the cladding. Both the cladded surface and HAZ are having lesser depth of indentation than the substrate.

The obtained values of nanohardness for the base is 4.53 GPa, for the interface 5.89 GPa and for the clad region 10.58 GPa. It is clear from the hardness values that the cladded area is having higher hardness compared to the base region. The HAZ hardness is lower than the cladded region due to the coarser structure. The observed hardness on the cladding surface was two times greater than the substrate. It is due to the formation of martensite and Fe content after the laser cladding, which is proved from the microstructure examination. The existence of Cr element in the cladding region gives an enhancement in toughness and corrosion performance.

Corrosion Test

Electrochemical corrosion tests were conducted in the presence of NaCl solution to understand the corrosion performance of the cladding. Potentiodynamic polarization curves were used to examine this corrosion behaviour. A Tafel plot is a polarization curve (typically logarithmic) that displays the connection among the current created in the cell and the electrode potential of a particular sample. Figure 3(b) shows the Tafel polarization curve for cladding at 0 h, 18 h and 42 h test durations. These positive-going potential (anodic-potential) profiles for various times express that the coating area is inactive to corrosion. Anodic potential increases the thickness of the passive film. Passive film is a thin oxide film with nanometre thickness, covered on the metal surface.
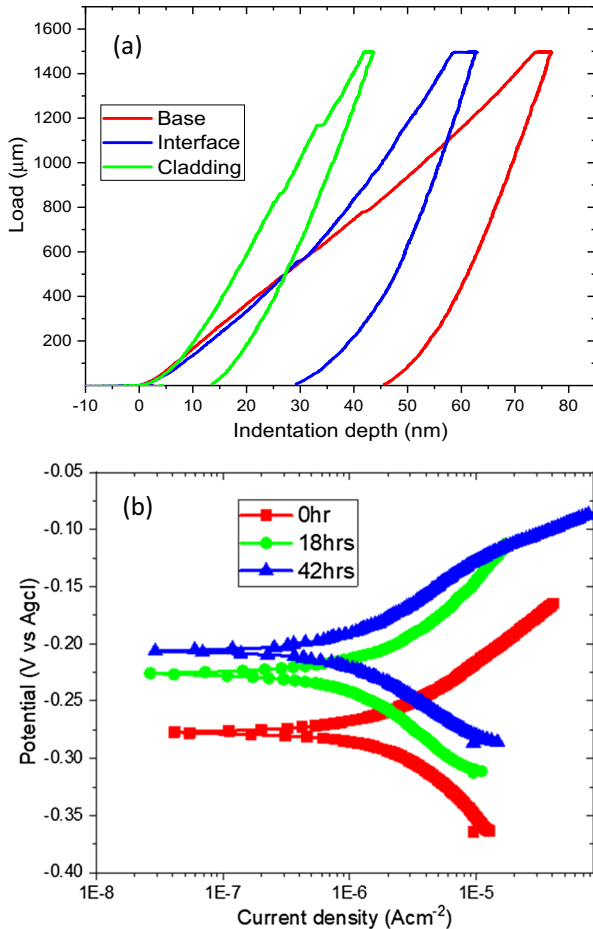
Fig. 3 (**a**) The indentation load-unloading profiles, (**b**) Tafel polarization curves

The extrapolated parameters are listed in Table 3. The obtained corrosion results indicate that at 0 h duration, the current density is 1.70134 A/cm^2, which is higher than the 18 h duration sample i.e., 0.75944 A/cm^2 and 42 h duration i.e., 1.2851 A/cm^2. The results explain that the corrosion current density at 18 h test sample is lower than that at 0 h and 42 h. The corrosion current density (I-current) is inversely proportional to the corrosion resistance of the test sample. Therefore, it is clear that the 18 h cladding specimen is providing the passive layer for long-time corrosion protection. Similarly, corrosion potential (E-current) indicates the chemical stability or corrosion potential of the sample. The potential of the sample is a point in Tafel plot at which the anodic and cathodic responses are kept in equilibrium. Corrosion usually happens at a rate determined by an equilibrium among opposite electrochemical responses. If the E-current is more negative, the samples are to be to corroded quickly. On the other hand, if E-current is lower negative or positive, the

Table 3 Corrosion test results

Test duration	I current (A/cm^2)	E current (V)
0 h	$1.70134295 \times 10^{-6}$	-0.277192982
18 h	$7.59442382 \times 10^{-7}$	-0.225891341
42 h	$1.28513697 \times 10^{-6}$	-0.204003962

sample are to be corroded minimum due to the passive layer formation. It is clear from the plots that the shift of E-current with an increase in test duration is towards the lower negative. These results indicate the concepts of continuous oxide layer formation and less porous structure. Moreover, it indicates that the corrosion potential is decreasing. While decreasing the corrosion potential, it indicates that the cladded specimen is started to get oxidizing and the negative charges are accumulating in it. The free of corrosion potentials is the absence of an electrical current which flows to and from a cladded surface. From these trends, it is clear that the cladded specimen can be improved the corrosion performance. Due to this reason, the I-current values were increased at 42 h duration as seen in Table 3.

Corrosion Morphology

The corroded morphology of the surface was used to envisage the concept of oxide formation. Figure 4 shows the corroded morphology and their corresponding EDS analysis after 0 h test duration. It is clear from the micrograph that there is minimum damage and initiation of oxide layer formation were observed on the corroded surface. The elements such as Cr, Fe and Oxide elements start showing up in the EDS result due to the initiation of the formation of oxides. Also, the oxide content is increased to 36.32%.
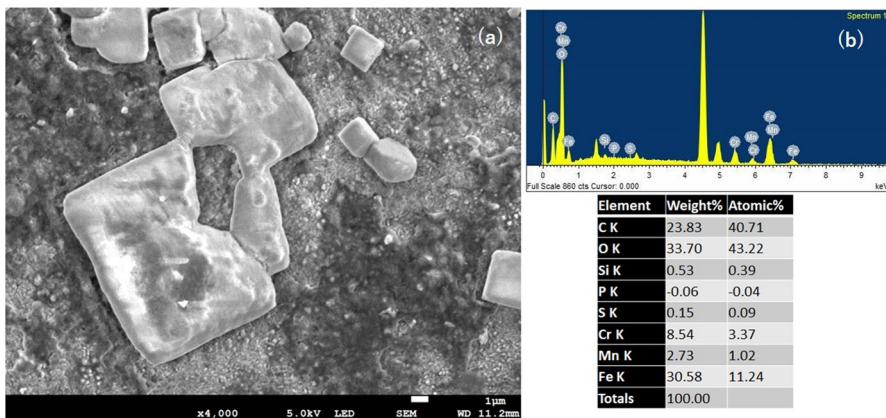

Element	Weight%	Atomic%
C K	23.83	40.71
O K	33.70	43.22
Si K	0.53	0.39
P K	-0.06	-0.04
S K	0.15	0.09
Cr K	8.54	3.37
Mn K	2.73	1.02
Fe K	30.58	11.24
Totals	100.00	

Fig. 4 (**a**) Corroded morphology at 0 h test duration, and their corresponding EDS results (**b**)

Figure 5 displays the corroded micrograph and their EDS analysis for 18 h test duration sample. It shows that a thick oxide layer was formed and a crystalline structure was discovered at the surface due to the presence of chromium. Peaks of Cr, Fe and Oxide elements in the EDS result indicate the formation of thick chromium oxide film on the surface. Stainless steel is one of the best corrosion-resistant alloys, which comprises at least 10.5% chromium. Chromium makes a self-curing oxide layer to bring corrosion resistance. The process of chromium-rich oxide film creation throughout the passivation progression can be comprehended with the following Eq. (1).

$$2Cr + 3H_2O = Cr_2O_3 + 3H_2 \tag{1}$$
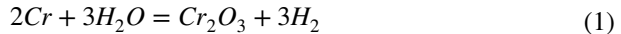
On the other hand, there is a significant drop of Fe & oxide in the 42 h EDS analysis. The reason for this is mainly because of the breaking of the brittle oxide layer, leaving the surface at some portions of the cladding. The element Fe content getting dropped to 3.65% is the key cause to lose bonding of generated oxide layers from the surface. Those detached patches are clearly observed in the SEM image in Fig. 6.

Electrochemical Impedance Analysis (EIS)

EIS method is largely used to study the corrosion performance of the materials. Figures 7(a-b) show the Nyquist and Bode plots of the laser cladding after 0 h, 18 h and 42 h of immersion in NaCl concentrated solution. The distorted semicircles in Fig. 7(a) are the Nyquist plots. Y-axis shows the impedance of the system, which is due to the coating capacitance in the circuit. The diameter of these semicircles denotes the resistance of the material to the charge transfer. Therefore, if this diameter is higher, the corrosion resistance of the material is higher. From the results, it is clear that the corrosion resistance of the cladding is increasing with time. This is due to less porosity, better microstructural consistency and oxide film formation. At
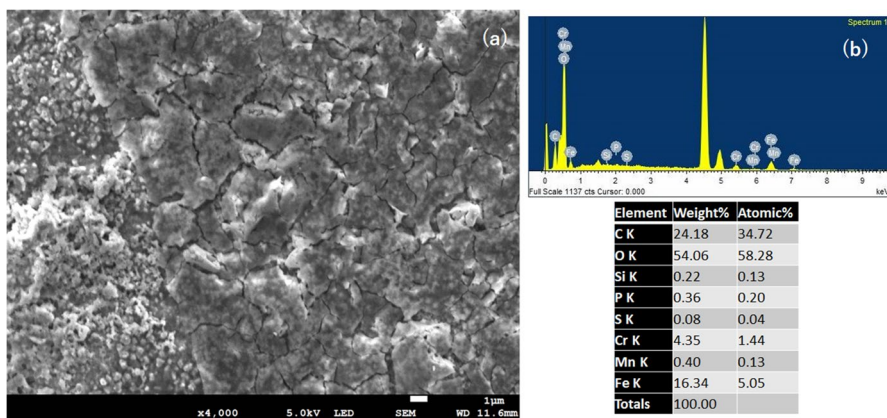

Element	Weight%	Atomic%
C K	24.18	34.72
O K	54.06	58.28
Si K	0.22	0.13
P K	0.36	0.20
S K	0.08	0.04
Cr K	4.35	1.44
Mn K	0.40	0.13
Fe K	16.34	5.05
Totals	100.00	

Fig. 5 (**a**) Corroded morphology at 18 h test duration, and their corresponding EDS results (**b**)
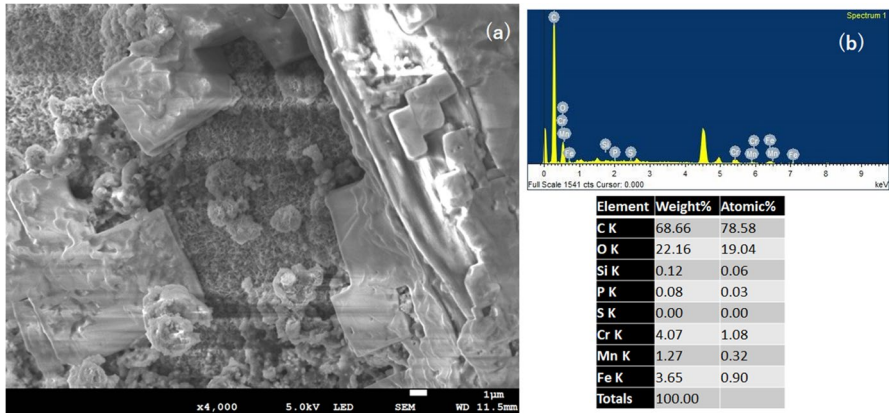
Fig. 6 (**a**) Corroded morphology at 42 h test duration, and their corresponding EDS results (**b**)
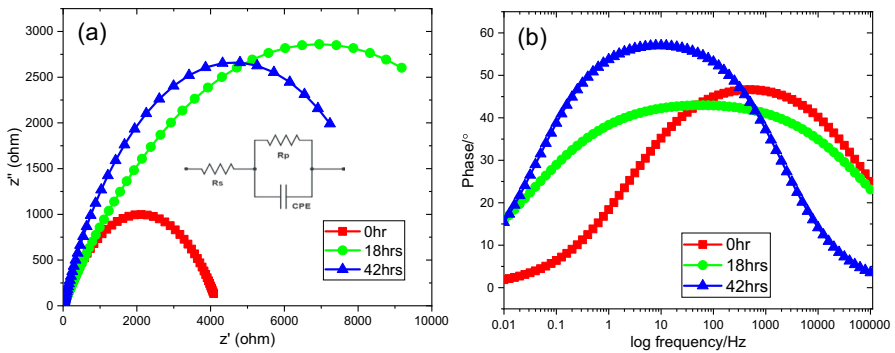

Fig. 7 (**a-b**) Nyquist and Bode plots obtained from the EIS analysis at various test durations, fitted electrical equivalent circuit included in (**a**)

42 h test time, a little drop in performance can be noticed. It is due to the breaking of the oxide layer. However, the diameter of this semi-circle is greater than the starting time (0 h). The Nyquist plot of all the test times contains a single capacitance curve, which is associated with the realization of a passive film.

Moreover, it is clear that the Nyquist plots obtained are not pure semicircles. It is due to the in-homogeneities of the electrode surface, which give frequency dispersion. It is a good practice to use equivalent circuit analysis technique for this kind of non-ideal response. As shown in the electrical equivalent circuit model inset in Fig. 7(a), the total impedance of the circuit depends on the solution resistance (Rs), pore resistance (Rp) and Constant Phase Element (CPE). Table 4 gives the values of Rp and CPE, which were obtained from the impedance plots and the equivalent circuit model. Having high Rp and low CPE is an indication of good corrosion performance. It is clear from the table that the 18 h cladded specimen is showing good corrosion performance during longer test times. Figure 7(b) shows the bode plots

Table 4 Values of Rp and CPE

Test duration	Rp (Ω)	CPE (μMho)
0 h	4187.2	660
18 h	13,876	161
42 h	9263.4	258

i.e., phase angle vs. frequency curve at various test durations. It is observed that, all three plots are having a single highest. It means that the corrosion takes place by the single charge transfer process, which is further confirming the discussion of the Nyquist plot. At the intermediate frequency region, the phase angle of all the curves is higher due to the passivation of the coating. Therefore, it is clear from this impedance study that the coating is providing a good corrosion resistance performance to the substrate.
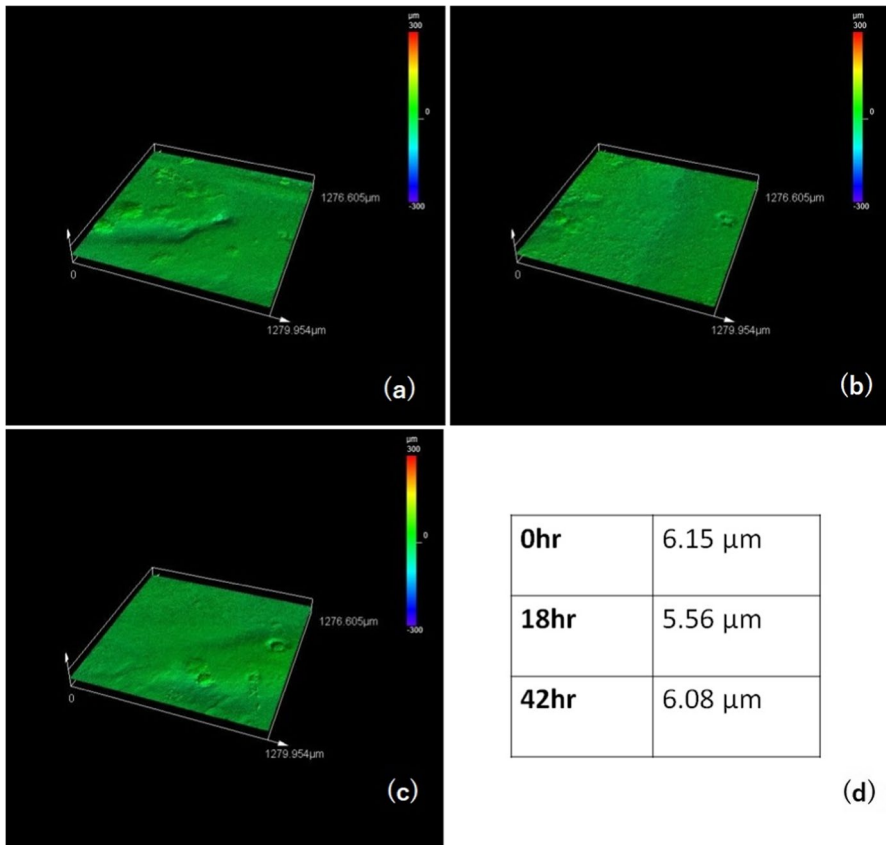

Fig. 8 Surface roughness measured through Olympus LEXT laser confocal microscopy: (**a**) 0 h, (**b**)18 h, (**c**) 42 h and their corresponding roughness values (**d**)

Roughness Examination

Surface roughness is a key representative of materials with useful requirements. The corrosion effect on the cladding surface was analysed by comparing the roughness values after corrosion. Figure 8 (a-d) shows the measured roughness of 3D plot with their values for various test duration samples. The roughness of the 0 h corrosion test is around 6.15 μm, which is higher than 18 h and 42 h test specimens. It is obvious that corrosion rate increases as well as the surface roughness of the cladded specimens also increased.

Then, the roughness values of the cladded surface were measured for the 18 h and 42 h test durations to analyse the corrosion rate. Figure 8(d) shows those roughness values. The 18 h corroded surface has a 5.56 μm roughness value, which is reasonably smaller than 0 h and 42 h test specimens. This declining trend points out that the corrosion rate is reduced due to enhanced resistance and smooth oxide layer. However, this surface roughness again increased to 6.08 μm due to the breakage of oxide layers from the surface.

Conclusion

In this study, the laser cladded SS420 particles on Ti-64 substrate was analysed in terms of microstructural, nanohardness, corrosion behaviour, and corroded roughness.

- The microstructure confirmed that the formed coating is dense, free from cracks and well adhered. The observed nanohardness on the surface of the cladding is two times greater than the substrate. This is because the cladding surface having Fe in martensite form can resist the surface from the outside applied load.
- The reducing corrosion potential trend over time has indicated the concepts of continuous oxide formation. Further, the micrograph and EDS results depict the oxide layer's morphology and the existence of chromium oxide film.
- EIS outcome indicated that, due to the thick oxide layer formation, the maximum corrosion resistance was obtained at 18 h test duration. However, at 42 h test time, the breaking of brittle oxide was identified because of the surplus formation of oxides with condensed Fe content.
- Surface roughness confirmed that the cladding with 18 h test specimen showed lesser roughness while compared with 0 h and 42 h specimens due to higher corrosion resistance.

Declarations

Competing Interest The authors declare that they have no known competing financial interests or personal relationships.

References

1. Welsch, Gerhard, Rodney Boyer, and E. W. Collings, eds. Materials properties handbook: titanium alloys. ASM international, 1993.
2. Murakami, T., et al.: Surface hardening treatment for CP titanium and titanium alloys in use of Ar–5% CO gas. ISIJ. Int. **46**(9), 1329–1338 (2006)
3. Reichelt, K., Jiang, X.: The preparation of thin films by physical vapour deposition methods. Thin Solid Films **191**(1), 91–126 (1990)
4. Gérard, B.: Application of thermal spraying in the automobile industry. Surf. Coat. Technol. **201**(5), 2028–2031 (2006)
5. Zhecheva, A., Malinov, S., Sha, W.: Titanium alloys after surface gas nitriding. Surf. Coat. Technol. **201**(6), 2467–2474 (2006)
6. Jeyaprakash, Natarajan, Che-Hua Yang, and Durairaj Raj Kumar. "Laser Surface Modification of Materials." Laser Ablation. IntechOpen, 2020.
7. Schaaf, P.: Laser nitriding of metals. Prog. Mater Sci. **47**(1), 1–161 (2002)
8. Vilar, Rui. "Laser alloying and laser cladding." Materials Science Forum. Vol. 301. Trans Tech Publications Ltd, 1999.
9. He, D., et al.: Improving tribological properties of titanium alloys by combining laser surface texturing and diamond-like carbon film. Tribol. Int. **82**, 20–27 (2015)
10. Vilar, R.: Laser cladding. J. Laser. Appl. **11**(2), 64–79 (1999)
11. Santo, L.: Laser cladding of metals: a review. Int. J. Surf. Sci. Eng. **2**(5), 327–336 (2008)
12. Shasha, L., Yuhang, W., Weiping, Z.: Microstructure and wear resistance of laser clad cobalt-based composite coating on TA15 surface. Rare. Metal. Mater. Eng. **43**(5), 1041–1046 (2014)
13. Lu, X.-L., et al.: Synthesis and characterization of Ni60-hBN high temperature self-lubricating anti-wear composite coatings on Ti6Al4V alloy by laser cladding. Opt. Laser. Technol. **78**, 87–94 (2016)
14. Jeyaprakash, N., et al.: Comparison of microstructure, mechanical and wear behaviour of laser cladded stainless steel 410 substrate using stainless steel 420 and Colmonoy 5 particles. J. Iron. Steel. Res. Int. **27**(12), 1446–1455 (2020)
15. Wang, K., et al.: Effect of molybdenum on the microstructures and properties of stainless steel coatings by laser cladding. Appl. Sci. **7**(10), 1065 (2017)
16. Jeyaprakash, N., and Che-Hua Yang. "Microstructure and Wear Behaviour of SS420 Micron Layers on Ti–6Al–4V Substrate Using Laser Cladding Process." Trans. Indian. Inst. Met. (2020): 1–7.
17. García-Rodríguez, S., et al. "Corrosion behavior of 316L stainless steel coatings on ZE41 magnesium alloy in chloride environments." Surf. Coat. Technol. 78 (2019): 124994.
18. Cabrini, M., et al.: Evaluation of corrosion resistance of alloy 625 obtained by laser powder bed fusion. J. Electrochem. Soc. **166**(11), C3399 (2019)
19. Feng, Kai, et al. "Corrosion properties of laser cladded CrCoNi medium entropy alloy coating." Surf. Coat. Technol. 397 (2020): 126004.
20. Shen, Faming, et al. "Effect of microstructure on the corrosion resistance of coatings by extreme high speed laser cladding." Appl. Surf. Sci. 517 (2020): 146085.
21. Nabhani, M., Razavi, R.S., Barekat, M.: Corrosion study of laser cladded Ti-6Al-4V alloy in different corrosive environments. Eng. Fail. Anal. **97**, 234–241 (2019)